JAAS

Routine high-precision Nd isotope analyses: An optimized chromatographic purification scheme

Journal:	*Journal of Analytical Atomic Spectrometry*
Manuscript ID	JA-ART-05-2021-000169.R1
Article Type:	Paper
Date Submitted by the Author:	01-Jul-2021
Complete List of Authors:	Hyung, Eugenia; California Institute of Technology, Geological and Planetary Sciences Tissot, François L.H.; California Institute of Technology, Geological and Planetary Sciences

ARTICLE

Routine high-precision Nd isotope analyses: An optimized chromatographic purification scheme

Received 00th January 20xx,
Accepted 00th January 20xx

DOI: 10.1039/x0xx00000x

Eugenia Hyung and François L. H. Tissot

High-precision Nd isotope measurements provide key constraints on the evolution of the silicate Earth and planetary bodies. As advances in mass-spectrometry and measurement techniques have brought the precision of $^{142}Nd/^{144}Nd$ measurements down to ±2 ppm (parts-per-million), systematic biases stemming from insufficient sample purification (matrix effects and/or isobaric interferences) or non-quantitative yields are becoming increasingly problematic. One of the most wide-spread approaches for Nd purification uses cation-exchange column chromatography with α-HIBA (2-methylactic acid) reagent. Despite its popularity, limitations pertaining to the level of purification and yield of the α-HIBA method exist. Here we present an optimized α-HIBA purification protocol that addresses these limitations and achieves the level of purity required for routine high-precision Nd isotope analyses. This protocol builds on existing methodologies and a comprehensive series of tests that we performed, and efficiently minimizes procedural blanks, the number of column passes, and thus the sample processing time, while maximizing recovery yields. We anticipate that this optimized protocol will benefit both established and new users of the α-HIBA column chromatography method.

Introduction

The ability to measure neodymium (Nd) isotope ratios at high precision is instrumental to the study of planetary formation and evolution. First, because the Sm-Nd system contains two radiogenic isotopes ($^{147}Sm \rightarrow {}^{143}Nd$, $t_{1/2}$ = 106 Byr; $^{146}Sm \rightarrow {}^{142}Nd$, $t_{1/2}$ = 103 Myr[1]), which are widely used in (i) geochronology[2–4], (ii) tracing mantle sources[5–7], and (iii) the study of the differentiation history of planetary silicate reservoirs[8–15]. Second, because Nd isotopes in solar system materials also display isotope anomalies of nucleosynthetic origin[16–20], which have recently brought critical insights into our understanding of early solar system dynamics[21–25]. The analytical challenge associated with resolving these isotopic signatures is variable. For ^{143}Nd excesses due to decay of ^{147}Sm, effects are typically quite large, at the epsilon level (*i.e.*, part per ten thousand deviations relative to the standard) and therefore readily measured with modern instrumentation. For ^{142}Nd excesses due to ^{146}Sm decay and nucleosynthetic anomalies, effects are much more subdued, typically resolvable only at the ppm to few tens of ppm level[10,26], and signatures are often close to the limit of resolution of state-of-the-art multi-collector mass-spectrometers[27]. As the precision of isotopic analyses are being pushed to higher levels, the question of measurement accuracy becomes paramount because systematic biases can start to affect the data outside of the stated uncertainties.

This concern is particularly important for $^{142}Nd/^{144}Nd$ ratios – a powerful tracer of silicate differentiation events occurring in the first 500 Myr of Earth's history – for which precision has now been brought down to ±2 ppm or better[11,27,28]. The confirmed presence[27,29] or absence of ±2–5 ppm anomalies in $^{142}Nd/^{144}Nd$ in the rock record in the past two billion years has important implications for constraining the timescales and vigour of mantle mixing throughout Earth's history[27]. At such level of precision, however, isotope fractionation during chromatographic purification due to non-quantitative yields, or incomplete separation of matrix elements/isobaric interferences could compromise data accuracy[28,30].

Here, we present an optimized protocol using alpha hydroxyisobutyric acid (α-HIBA; also often called MLA or 2-methylactic acid) as an eluent on a cation exchange resin (AG50-X4). We show that this method simultaneously fulfils the requirements of Nd purification and near-quantitative yield while minimizing the number of column passes, and thus the sample processing time and blanks. The reproducibility and robustness of the separation is tested using both multi-elemental standard solutions and reference material (*e.g.*, BHVO-2) powder digests. High precision (±2-5ppm) data obtained on the purified samples demonstrates the lack of systematic biases introduced by this protocol. To allow easier replication of our optimized methods, the full details on the experimental setup is provided in the paper and Supplementary Materials (including SolidWorks drawings of the columns and other custom-made parts, available for download at www.isotoparium.org).

Background

Neodymium is part of a family of fourteen refractory lithophile elements called Rare Earth Elements (REEs). They are known for their near identical geochemical behaviour, which stems from (i) their very

The Isotoparium. Geological and Planetary Sciences Division, California Institute of Technology, 1200 E California Blvd, Pasadena CA 91125. E-mail: ehyung@caltech.edu and tissot@caltech.edu

Electronic Supplementary Information (ESI) available: [details of any supplementary information available should be included here]. See DOI: 10.1039/x0xx00000x

similar ionic radii, and (ii) the fact that most of these metal ions exist primarily in the trivalent oxidation state in geological samples (Eu and Ce can also exist as Eu^{2+} and Ce^{4+}, respectively). These characteristics make the separation of the individual members of the REEs especially difficult, and the task has even been called "*one of the greatest challenges in the separation of metal ions*"[31]. Although a variety of approaches have been developed for the bulk separation of REEs[31], high-precision isotopic analysis of Nd (or any REE), generally involve a multi-step chromatographic purification whereby a primary column is used for matrix removal (*i.e.*, REE pre-concentration), and a secondary column (or series of columns) for individual REE separation. The goal is, while ensuring near-quantitative recovery yields, to remove any matrix element or critical isobaric interference (*e.g.*, ^{142}Ce, ^{144}Sm), which could affect the accuracy of high precision data.

The REE pre-concentration step is typically performed using a cation exchange resin, loading the sample in a reagent where major elements have little affinity for the resin, while the REEs and some other traces elements (*e.g.*, Ba) are initially retained and eluted after all major elements. The purification of Nd from the other REEs is where the challenge resides and significant improvements can be made. Two main purifications techniques are commonly used in the literature. (i) The first method, often called α-HIBA chemistry, uses α-HIBA as an eluent on a cation exchange resin (*e.g.*, AG50-X4) [2,3,8,9,17,19–22,25,27,30,32–87] to elute REEs in order of increasing atomic number. This method provides good separation of Nd from other REEs, but suffers from several limitations pertaining to the exact experimental setup. To achieve proper Nd separation, long and thin glass columns are used (L=20–30 cm, ø=1–2 mm), which need to be calibrated for each new batch of α-HIBA, and sporadic low yields and residual Ce and Sm in the Nd cuts have been reported. (ii) The second separation method, often called the $NaBrO_3$ or oxidative method, uses the Ln-Spec extraction chromatography resin where HDEHP (hexyldiethyl hydrogen phosphate) acts as the resin extractant phase and nitric or hydrochloric acid as the mobile phase[11,13,19,25,30,50,60,64,68,71,74,79–81,85,88–111]. On this resin, REEs elutes in order of decreasing atomic number, and Ce is efficiently removed by oxidation to Ce^{4+}, which complexes with HDEHP and does not elute. The attractiveness of this approach is that it achieves good Nd separation and consistently good yields (80-100%), and the setup is easy to implement (no recalibration with each acid batch). This method has its drawbacks too as non-quantitative yields result in ppm magnitude nuclear field shifts effects[28], and residual Na, Br and Ba must be removed through an additional clean up chemistry on cation exchange resin.

Recently, two important variations have been proposed to address some of the limitations of the main methods presented above. The first one is the use of high performance liquid chromatography systems (HPLC) for the Nd separation step[15,28,101,112,113]. Indeed, as thinner and longer columns yield better separations but their flow is prohibitively slow when driven by gravity alone, column pressurization is an attractive solution. However, handling of the harsh reagents used in the Ln-Spec chemistry requires a metal-free flow path, which most commercial HPLC system lack. To date, only two systems have been successfully used for separation and high precision analysis of Nd isotopes, the ESI Prep*FAST*[15,28,113] and a one-of-a-kind fluoropolymer HPLC prototype[101,114]. The clear advantage of these systems is the purity of the separation they produce, while their clear disadvantage is their high cost, which is a limiting factor for broad adoption by the community. The second development involves a series of specialized extraction chromatography resins (DGA-LnSpec-TruSpec), used in a sequence of three tandem steps allowing for Nd purification without the need for any collection or evaporation step[115]. This method successfully minimizes blanks and sample processing time, but also suffers from some limitations: it is not adapted to the processing of large amounts of depleted samples for routine Nd analysis on the TIMS, and reported yields are only on the order of 80 to 90%.

Regardless of the method used, the end goal is always the same: obtaining with minimal effort a sufficiently purified Nd cut to ensure accurate and precise isotope analysis. As such, an optimal scheme would minimize the number of column passes to ensure a short sample processing time and low blanks, while simultaneously providing near-quantitative (*i.e.*, close to 100%) recovery yields to alleviate any concern of fractionation during column chemistry. Here, we present developments in α-HIBA chemistry, which address the main limitations of this method highlighted above. Our optimized separation procedure consists of a three-step chemistry, which achieves consistently high total recovery yields (>95 %), and results in negligible isobaric interference levels (Ce/Nd < 1 ppm and Sm/Nd ~ppm-level). To streamline implementation in other laboratories, we provide a detailed description of all aspects of the analytical set up, including SolidWorks drawings of custom-made components.

Methods

In order to optimize Nd purification using α-HIBA chemistry, we systematically assessed and refined each step of the process. A step was found to be improved if, all else being equal, a particular modification led to higher recovery yields, higher purity of the Nd cut, lower processing time and/or lower blanks. Here and throughout the paper, the term "recovery yield" refers to the ratio of number of atoms recovered in the Nd cut over the number of atoms loaded onto the column. The recovery yield of a given step might be less than 100% if (i) some Nd stays bound to the resin (*i.e.*, does not elute), or (ii) some Nd elutes outside of the Nd cut fraction. The "total recovery yield" of the whole chemistry, is the product of the yield of all individual steps. All experiments and analyses were conducted at the Isotoparium (Caltech).

Sample dissolution

Rock powders (~100 mg) were placed in clean 7 ml Teflon beakers and dissolved by acid attack on hot plate using 4 ml of HF/HNO_3 (3:1) at 180°C for three days. The samples were then evaporated completely and redissolved into 3.5 ml of aqua regia (HCl/HNO_3, 3:1) at 160°C for three days. After this step, the samples are typically digested, and completely dried down again before being redissolved in 1.5 M HCl (3 ml for every 100 mg of sample).

REE pre-concentration chemistry

In the literature, this step typically uses cation exchange chromatography with HCl as the eluent[36,39,40,52,57,87]. Sample loading utilizes high purity 1.5 M HCl, while major element elution up to Sr utilizes high-purity 2.0 M (refs. 33,40,47,87) or 2.5 M HCl (refs. 17,39,53). Higher molarity HCl (4.0–6.0 M) is finally used to release the REE from the resin. Variable column dimensions have been used, including long, custom-made columns (L=20–26 cm, ø =0.6–1 cm)[70,78,109], to improve the resolution of the separation.

Here, the REE pre-concentration step is performed on mass produced poly-propylene R1010 columns (Environmental Express®, ø =9.3 mm, 5.5 mL capacity), fitted with HDPE frits (45–90 µm porosity). The high-density polyethylene frit is provided with the poly-propylene columns, and its size is manufactured to fit in the inner diameter of the column. This particular column was chosen for its high-capacity reservoir, low cost, ease of acquisition, and likely long-term availability, minimizing the chance for future recalibration due to product discontinuation. The columns, frits, and reservoirs were cleaned by soaking them in a bath of 6 M HCl (reagent grade) for three days, then subsequently soaked in a bath of 3 M HNO_3 + 1 M HF (reagent grade) for three days. The resin used during this step, AG50W-X8 (100-200 mesh size) was cleaned with one resin volume of ultra-pure 3.0 M HNO_3, one resin volume of MQ water, then one resin volume of ultra-pure 4.0 M HCl, and finally rinsed with three resin volumes of MQ water. The resin was loaded onto the column, conditioned in up to 50 mL of 4.0 M HCl (or until there is no change in resin volume), and the resin height adjusted to the neck of the column where the column first begins to widen into the funnel-holder (~8 cm height).

For loading/rinse/REE elution, double-distilled HCl of three different molarities (~1.5 M, ~2.0 M, and 4.0–6.0 M HCl) have typically been employed. Various combinations were tested (*i.e.*, 1.5/1.8/3.6 M HCl; 1.5/2.0/4.0 M HCl; 1.5/2.5/4.0 M HCl) in order to derive an optimal elution scheme for this step (see results and Table 1).

Nd purification from other REE

Nd separation from other REEs using α-HIBA chemistry typically involves the use of long and thin columns (L= 20–30 cm, ø=0.1–0.2 cm) and 0.10–0.25 M α-HIBA as the eluent, calibrated to a pH of 4.1 to 4.8 (refs. 39,40,64,83,87). Both AG50W-X4[40,45] and AG50W-X8[57,87] cation exchange resins have been used, and since a gravity-driven drip set-up greatly increases the duration of an elution, the columns are often pressurized and timed[22,27,78,116].

Here, the α-HIBA chemistry step was performed using 0.2 M α-HIBA (MilliporeSigma), calibrated to a pH of 4.62 (±0.03) using NH_4OH solution (Optima grade), and AG50W-X4 cation exchange resin (200-400 mesh size) in NH^{4+} form. As α-HIBA solutions tend to stick to plastics (including fluoropolymers, such as PFA/PTFE), and to a lesser extent quartz, custom-made borosilicate glass columns with ~15 mL reservoirs (OD = 25 mm) were used.

The column capillary internal diameter was 2 mm (OD = 5mm), and as longer columns provide better separations between peaks, two different column lengths were tested: 30 cm and 60 cm (resin height). The columns were pressurized (0.35 psi) using high-purity compressed air supply and a low-pressure regulator (Fairchild). To ensure pressure homogeneity when running several columns in parallel, the pressurized air was split into multiple channels using wye connectors and flexible PVC tubing of equal length.

For each column, a holder, whose design was adapted from the Sm-Nd separation column set-up used in G. J. Wasserburg's lab, was machined out of ultra-high molecular weight cylinder. The top and bottom caps of the column holder, built out of polypropylene, secure the glass column from above and below (see SolidWorks drawings). At the bottom of the glass column, a Teflon nozzle (holding a frit) is placed between the borosilicate column and the bottom cap, to guide the eluate out of the column without contact with the cap. Below the nozzle, a commercial infrared drop-counter (NEULOG) keeps track of the eluted volume collected. Column holders and drop counters are secured to a stand, so they can be moved as a single unit. The frits (35-µm porosity, single use) were cut out of filter paper (*e.g.*, Whatman) to the size of the outer diameter of the column, cleaned with 4 M HCl at room temperature for one hour, before being rinsed and soaked in MQ water for one day and air-dried in a laminar flow hood.

The elution protocol followed a typical isocratic elution with 0.2 M α-HIBA at pH = 4.62±0.03 on AG50W-X4 (Table 1). The pH of the α-HIBA solution was originally modified from Gd-Sm separation chemistry[117,118] for ease of separation for lighter rare earths such as Nd[2,34,39]. The resin was conditioned with ~7 mL of 0.2 M α-HIBA overnight in an unpressurized state prior to sample loading. To improve Ce removal, the REE fraction from the matrix removal chemistry step was dried down to ~1 mL and treated with 200 µL of 30% H_2O_2 (Optima grade). The beaker was capped and set on a hot plate at 80–90°C overnight to oxidize Ce to Ce^{4+}. The cut was then dried down completely at 90 °C, redissolved in 75 µL of 0.75 M HCl, and loaded onto the α-HIBA column. An additional 75 µL was added to the beaker to recover any residual sample, before loading onto the column (150 µL total loading volume). To prevent diffusion of the sample back into the reservoir in subsequent steps, a small amount of α-HIBA was loaded onto the capillary in two aliquots (~80 µL each). The column reservoir is then filled with ~7 mL of α-HIBA solution, and the column is continuously pressurized at 0.35 psi until the end of the elution. This step is repeated twice to further remove other REE from the Nd cut.

To optimize this chemistry, two main types of tests were conducted. First, the performance of a 60-cm column was compared to that of a 30-cm column to see if a single column pass could produce a Nd cut sufficiently clean (*i.e.*, removal of isobaric interferences). A single column pass would be advantageous, helping to decrease blanks and sample processing time. Second, several elution conditions that could affect the yields were systematically modified and their impact of the yields assessed. These were (i) the elution rate, as controlled by the amount of column pressurization, (ii) the stability of the column pressurization, and (iii) the nozzle geometry, which impact the back pressure and drop size.

Mass spectrometry

Calibration and elution curves for the matrix removal and α-HIBA columns were performed with 1.00 mL of 100 ppb REE solutions (SPEX CertiPrep CLMS-1 multielement solution), equivalent to 100 ng of Nd (and all other REEs), which was dried down and redissolved into 0.75 M HCl. For elutions, small aliquots (referred to hereafter as "column tails"), were collected before and after the cuts in order to monitor the consistency of the calibrations, and to assess whether a loss in yield could be attributed to a shift in calibration. For the matrix removal step, this is ~3 mL before and after the cuts, and for the α-HIBA elution step, ~4 drops before and after cuts. Rock samples (BHVO-2, Columbia River Basalt) are used in a separate set of elutions to check for consistency when using natural sample.

All analyses were performed at the Isotoparium. Concentration measurements for calibrations and elution curves, as well as purified cuts and column tails were performed on an iCAP-RQ (ThermoFisher) Quadrupole ICP-MS, while high-precision Nd isotope analyses were conducted on a Triton (ThermoFisher) TIMS.

To build an elution profile, fractions were collected in 3-mL increments for the pre-concentration chemistry step, and 4-drop increments for the REE columns. For yield assessments, the entire fraction expected to contain Nd was collected as a single cut, along with elution tails, before and after this cut, and the amount of Nd in these fractions was compared to that contained in the initial load (1 mL of 100 ppb SPEX CertiPrep CLMS-1 multielement solution). All collected fractions and the newly prepared initial load, were dried-down into 5 mL Teflon beakers, redissolved in 5 mL of 3 % (vol) HNO_3 and run on the iCAP-RQ. The instrument was run in STD mode, with nebulizer and auxiliary gas flow rates set at 1 and 0.8 L/min, respectively. Signal sensitivity and stability were optimized using the iCAP Q/RQ tuning solution (ThermoFisher Scientific) containing 1.0 ppb Ba, Bi, Ce, Co, In, Li, and U in 2% HNO_3 and 0.5% HCl. Calibration curves for REEs were built by measuring gravimetric multi-elemental solutions (obtained from SPEX) spanning a range of concentrations from 1 to 10 ppb. To monitor instrumental drift throughout the analytical session, a 2 ppb Ho solution was measured every four samples. To achieve a higher degree of precision in assessing yield, a 10 ppb In internal standard was employed to correct for instrumental drift[119].

Isotope ratio measurements were performed with a Triton thermal ionization mass spectrometer (TIMS) and double Re filaments. Prior to sample loading, one microdroplet (~0.15 µL) out of 1.0 µL of 0.17 M H_3PO_4 was loaded onto the evaporation filament (zone-refined Re filament, >99.995%, H. Cross Co, Moonachie, N.J., USA). The sample, corresponding to ~1 µg of Nd, was dissolved in 1 µL of 3 N HNO_3 and then mixed with the remainder of the H_3PO_4 (0.85 uL) to be loaded onto the evaporation filament in no less than a total of 10 increments with a 0.5–3.0 µL capacity pipette (Sartorius). Neodymium isotopes were analysed as Nd^+, using a dynamic $^{142}Nd/^{144}Nd$ method adapted from Hyung and Jacobsen (2020) (ref. 27). The method, initially developed on an Isotopx IsoprobeT, was adjusted to the Triton TIMS. Owing to the difference in the distribution and number of faraday cups between the two instruments, the beams were arranged as shown in Table 2 with ^{140}Ce collected in the lowest cup (L4) and ^{148}Nd in the highest cup (H4) in the main sequence, while ^{150}Nd was collected in the second sequence. Between each block consisting of 10 cycles, the amplifier rotation function was used to cancel gains. Data was collected in multiples of nine blocks to cancel differences in gains across the nine amplifiers assigned to the nine Faraday cups. The number of cycles for each measurement ranged from 360 to 1260 (Table 5), with an integration time of 8.389 seconds and a magnet idle time of 3 seconds, corresponding to a run time of ~4 to 11 hours. After correcting for isobaric interferences, raw isotope ratios were corrected for mass fractionation to $^{146}Nd/^{144}Nd=0.7219$ using the exponential law. We report static measurements for all other Nd ratios.

Results

REE pre-concentration chemistry

Figure 1 shows the optimal elution curve, obtained using 3 mL of 1.5 M HCl per 100 mg of sample for sample loading, 3 mL of 1.5M HCl and 55 mL of 2.0 M HCl for elution of the major elements in and 36 mL of 4.0 M HCl for elution of Nd (including column tails). The same elution volume applied even when loading of a 300 mg sample in 9 mL of 1.5 M HCl. The elution, including resin cleaning and conditioning, takes about four hours to complete, and 6 to 12 samples can easily be processed in parallel. The recovery yield of Nd for this step was found to consistently be 99%, both with multi-elemental solutions and basaltic geostandard. Other acid combinations tested provided either no improvement in separation while using larger acid volumes or poorer separations (see Supplementary Materials).

α-HIBA chemistry

For the α-HIBA chemistry, elutions are reported in terms of the number of "drops" passed through the column. Each drop was ~45–50 µL in volume, where volume variability stems from minute differences in the inner diameter of the column, flow rates, and the shape of the Teflon nozzle fitted at the tip of the column. Whereas the drop size is typically uniform for a singular drop rate on a given same column, calibrations of different columns differed by 5–25 drops Although this requires a careful calibration of each column independently, such a process is only needed once for a given column, as elutions were found to be highly reproducible (Figure 2).

Our tests in the α-HIBA chemistry reveal several factors, which can affect the Nd separation. Most importantly is the eluent flow rate, which is imposed by the amount of pressurization applied at the column head, and which was found to have a very significant impact on both the position of the elution peaks and the recovery yields. Figure 3 shows the elution peaks for Sm and Nd for two elutions conducted under otherwise identical conditions (*i.e.*, 30 cm column, 35 µm porosity frit), but with two different flow rates: ~50 µL/min (1.0 psi of head pressure), and ~29.9 µL/min (0.35 psi of head pressure). In the faster elution, peaks elute early by 4 to 6 drops (~0.2 to 0.3 mL) relative to the slower elution, and the recovery yield of Nd were, respectively,

only 93%, against 98% (Table 3). An important consequence is the improvement in the separation of Pr from Nd. At a flow rate of 50 µL/min, two passes through the α-HIBA column reduced the original amount of Pr in the Nd cut to 5%. In contrast, >99% of the Pr was removed after two α-HIBA column passes when changing the pressure conditions on the column from 1.0 to 0.35 psi (29.9 µL/min) (Table 4).

The consistency of the column pressurization was also found to impact the α-HIBA chemistry. Figure 4 compares an elution (labelled "*Reference*") in which no disturbance (*e.g.*, shock or movement) affected the flexible PVC tubing used to bring the compressed air to the column head, with another elution (labelled "*Unstable*") where the tubing was purposely moved early in the elution (~100 drops after sample loading). Relative to the "*Reference*" elution, a significant drop in yield was observed in the "*Unstable*" elution: from 93 to 78%.

The impact of column length and geometry was also found to be significant on the quality of the separation and recovery yields. In one instance, a column nozzle, machined to flare outward (Figure 5a; top right corner), was used during a calibration curve test. The resulting elutions are shown in Figure 5a and c). Although the general profile (Figure 5a) looks similar to that obtained with a properly shaped nozzle (Figure 5b), the peak positions were affected (earlier elution). More importantly, inspection of the elution peak on a logarithmic scale revealed concurrent release of supposedly already eluted elements with each new element (*e.g.*, Sm with Nd and Ce, and Nd with Ce; Figure 5c vs 5d).

Extending the length from 30 to 60 cm was also tested to determine if a single column pass on a longer column could provide as good a removal of isobaric interferences as two passes on the 30 cm column. As for the 30-cm column, the eluent flow rate had a pronounced impact on the recovery yield. At 50 µL/min (2.2 psi), the Nd yield was only 70% on the 60-cm column. This value increased to 97% after the flow rate was adjusted to 39.5 µL/min (1.5 psi) (Table 3), resulting in an elution time of 4.4 hrs for Nd, vs 3.3 hrs for the high yield elution on the 30-cm column (~30 µL/min, 0.35 psi) (Table 2). At the flow rates needed to achieve >97% Nd yield, the use of a 60-cm column reduced the Ce/Nd and Sm/Nd ratio in the Nd cut to 0.15 and 0.65%, respectively, similar to a single pass on a 30-cm column. Only the separation of Pr from Nd was markedly improved on a 60-cm column, where the Pr/Nd ratio was reduced to 0.001 from 1.0, compared to 0.03 from 1.0 on the 30-cm column (Table 4).

One or two passes on an α-HIBA column?

Using the multi-REE solution from SPEX, a single pass on a 30-cm α-HIBA column reduced the Ce/Nd and Sm/Nd from unity to ~(1-3) × 10^{-3}. Removal of Ce from Nd was improved by a factor of 20 when having treated the sample with H_2O_2 once, prior to loading the sample onto the α-HIBA column (Table 4). These values indicate that two steps of α-HIBA chemistry can achieve lower than 1 ppm interference on (i) ^{142}Nd from ^{142}Ce, even for samples with Ce/Nd as high as ~500, and (ii) ^{144}Nd from ^{144}Sm for samples with Sm/Nd ratios of about 0.6 (*i.e.*, ~2x the chondritic values) (Table 4). Interference levels observed on processed rock samples (*i.e.*, BHVO-2, BCR-2) are consistent with these expectations and reported in Table 5.

While the use of a 60-cm column provides some separation improvement relative to a 30-cm column, the truly significant separation gain comes with two passes of the sample through the α-HIBA chemistry, and we thus favor the use of a 30-cm column, which provides a more compact and easier to handle setup.

Blanks

For a Nd purification involving one REE pre-concentration chemistry step and two passes on the α-HIBA columns, the Nd blank was found to be between 45-55 pg, a value negligible compared to the amount of Nd needed for high precision analyses (~1 µg).

Nd isotope data

The high-precision precision Nd isotope data obtained for one geostandard (BHVO-2) and one terrestrial sample (Columbia River Basalt) is given in Table 5. The data is in excellent agreement with literature data[22,27,28,30,83,95,115] (Figure 6). In particular, the ^{142}Nd/^{144}Nd ratios of the samples were found to be identical to the JNdi-1 standard, within 2σ=±2-5ppm. In addition, the measured ^{143}Nd/^{144}Nd, ^{145}Nd/^{144}Nd, ^{148}Nd/^{144}Nd, and ^{150}Nd/^{144}Nd ratios deviations from JNdi-1 for the Columbia River Basalt (BCR-1, BCR-2) and BHVO-2 are in close agreement with literature data[22,28,30,83,95,115].

Discussion

Achieving consistently high yields

One of the main perceived weaknesses of the α-HIBA chemistry is the non-reproducibility of the Nd yields, which have been reported in the literature to vary between 60 and 100%. Our results demonstrate that consistently high yields (>95%) and good separations can be achieved provided the eluent flow rate is not too high and the pressurization conditions remain stable throughout the chemistry.

These observations naturally fit into, and can readily be explained using, the theory of chromatography. According to the plate theory introduced by Martin and Synge (1941) (ref. 120), a chromatographic column can be modelled as a series of plates of identical heights, within which the analyte distribution between the liquid and solid phases is assumed to reach instantaneous equilibrium. The lower the Height Equivalent to a Theoretical Plate (HETP), the greater the number of plates in the column, and therefore, the narrower the elution peaks and the better the separation. Physically, three main factors control the HETP: (i) the variability of eluent flow paths within the column, which depends on the resin particle size, size distribution, shape, and bed structure, (ii) the longitudinal diffusion of the analyte within the mobile phase, and (iii) resistance to mass transfer, whereas in practice, analytes in the solute take some time to reach, bond to, and then leave the solid phase. As such the HEPT if often described as the sum of three terms (van Deemter equation):

$$HETP = Hp + Hd + Hm \quad (1)$$

The first term, *Hp* is the HEPT component due to the variability of flow paths, and can be described as $Hp = 2\lambda d_p$, where *dp* is the

particle diameter, and λ, a coefficient that depends on the particle size distribution (close to 1). For a given resin, *Hp* is constant value with no dependence on flow rate. The second (*Hd*) and third term (*Hm*) describe the HETP contribution from, respectively, longitudinal diffusion and mass transport. These can be described as a function of the eluent flow rate by:

$$H_d = 2\frac{\gamma D_m}{v} \quad (2) \quad \text{and} \quad H_m = \omega\frac{d_p^2}{D_m}v \quad (3),$$

where γ is a diffusion restriction factor, D_m the diffusion coefficient of the analyte in the mobile phase, ω, a coefficient describing pore size distribution and shape, as well as particle size distribution, and *v*, the velocity of the eluent in the column. Equation 1 can be rewritten to highlight the dependency on eluent flow rate as:

$$HETP = A + B/v + Cv \quad (4).$$

The minimum HETP is achieved for $v = \sqrt{B/C}$. At lower flow rates, longitudinal diffusion will increase plate height, which will decrease the degree of separation achieved. At higher flow rates, the eluent is moving too rapidly for the analytes to uniformly penetrate the resin and achieve equilibrium[121], which will also decrease the quality of the separation and the yield (without time for equilibration, a portion of the analytes bound to the resin might not get released).

Figure 7 shows the HETP obtained on the 30-cm column for the three elutions rates tested in this study, and three possible fits through the data using Eq 4. The higher HETP obtained at higher flow rates (Figure 7) indicates that equilibrium is not fully achieved in the column, which is the most likely explanation for the low yields observed at such flow rates (Table 3). As such, pressurizing a column or using a vacuum box to increase the flow rate of the α-HIBA chemistry (and anion/cation exchange chemistries in general), will eventually compromise yield, or the quality of separation by broadening elution peaks. Acceptable fits of Eq. 4 through the data allows to derive the minimum HETP achievable for this α-HIBA chemistry configuration (*i.e.*, the *Hp* term in Eq. 1, and *A* term in Eq. 4) as ~0.50–0.75 mm. This in turn, provides a means to determine an optimal elution speed (and thus column pressurization). At face value, the gravity driven elution (which takes 6.5 hr, flow rate of ~15 µL/min) achieves an HETP closest to the minimum achievable HETP and would result in a higher yield than pressurized columns. Yet, the still very high yield (>98%) and shorter elution time (3.3 hr) of the lower pressure elution (0.35 psi, flow rate of ~30 µL/min) makes it a more attractive configuration to ensure high-precision data (at the ±2ppm level), while minimizing sample processing time.

It is not only the eluent flow rate that can impact the separation and yields, but also the consistency of the flow. As shown in Figure 4, disturbances to the pressurizing tubing during the elution can result in lower yields, highlighting the importance of maintaining constant elution conditions to achieve high yields. Mechanistically, the observation of lower yield when pressurization conditions vary during the elution might be explained by changes in the eluent flow paths throughout the resin, resulting in the isolation of resin domains that have already bound to some of the analytes, which can no longer be released into the flowing eluent as the chemistry proceeds.

Although there have been reports of variable Nd recovery yields when using α-HIBA chemistry[22,30], as low as 60%, we show here that consistently high yields can be achieved with slow, stable elutions conditions that (i) allow resin-eluent equilibration, and (ii) avoid sudden flow path modifications. Indeed, given the recovery yield of 99% measured for the matrix-removal step, and the 98.5 % yield for a single pass on the α-HIBA column (at a drop rate of ~30 µL/min), a routine total recovery yield of ~95% is achieved using the optimized protocol presented here, (*i.e.*, one matrix removal step + two α-HIBA steps). This value is similar to the highest yields reported for the triple tandem columns[115], and $NaBrO_3$/oxidative[30] methods.

Achieving high quality Nd separation

Near quantitative yields are necessary but not sufficient to ensure the accuracy of high-precision data, owing to the impact of potential matrix effects (*e.g.*, from residual major elements, Pr) and/or isobaric interferences (*e.g.*, from ^{142}Ce or ^{144}Sm for ^{142}Nd/^{144}Nd analyses).

Comparisons of different molarity acids (1.8 M vs 2.0 M vs 2.5 M HCl/3.6 M vs 4.0 M HCl) for the matrix removal step demonstrated that small changes in acid molarity led to relatively large changes in elution volumes. For instance, using 3.6 M HCl for the elution of REE compared 4.0 M required an extra 15 mL (50% increase) to fully elute Nd (Supplementary Materials Figure S1). Similarly, using 1.8 M HCl for the matrix removal step instead of 2.0 M HCl increased the amount of HCl to be eluted for this step by at least 30 mL. We find that near quantitative removal (>99 %) of matrix elements can be achieved most efficiently using 55 mL of 2.0 M HCl (Figure 1). At this molarity, REEs are efficiently retained unto the column until their release using 4.0 HCl (Nd is collected into 36 mL, including column tails).

As major elements are efficiently removed by the REE pre-concentration chemistry, the main concern in terms of matrix effect comes from praseodymium (Pr), a monoisotopic element (atomic mass of 141). The impact of Pr on high precision Nd isotopes in general, and ^{142}Nd/^{144}Nd in particular, is low. Praseodymium does not directly cause isobaric interferences onto ^{142}Nd, and tailing effects of large ^{141}Pr beams have been shown to have negligible effect on ^{142}Nd/^{144}Nd ratios in TIMS analyses[30]. Yet the production of hydrides (PrH) may be a concern for ^{142}Nd/^{144}Nd measurements on MC-ICPMS,[28] making Pr removal an important part of a successful Nd separation scheme. Specifically, Saji et al (2016) (ref. 28) found that ^{141}Pr/^{142}Nd ratios below ~0.2 were needed for accurate MC-ICPMS analyses. Our procedure removes 97% of the Pr with each pass on the α-HIBA column, such that less than 1 permil of the initial Pr makes it to the purified Nd cut after two column passes (Pr/Nd ~2×10^{-4} from Pr/Nd=0.22; Table 4). The efficiency of Pr removal of our method is comparable to the tandem separation methods of Pin et al., (2019)[115] (Pr/Nd ~low 10^{-4} starting from Pr/Nd =0.22), and a vast improvement compared to the oxidizing method involving $NaBrO_3$[30] (Pr/Nd<0.05 from Pr/Nd=0.22), or fluoropolymer HPLC systems[28,101] (Pr/Nd ~1×10^{-2} from Pr/Nd =0.22 in ref. 28; significant overlap of Pr and Nd elution peaks in ref. 101).

More than the removal of Pr, the main advantage of the α-HIBA chemistry may be in the quality of Ce separation (Table 4). Owing to

the order of REE elution, only ~1 permil of the initial Ce make it into the Nd cut in a single column pass, yielding at most low ppm levels of Ce in the final Nd cut (Table 4). The addition of H_2O_2 to a sample, promoting the oxidation of Ce^{3+} to Ce^{4+}, further improves the separation, which is particularly beneficial for samples with high initial Ce/Nd ratios, such as for carbonatites or granites (Table 4 and 5). Processed samples all show sub-ppm ^{142}Ce interference level on ^{142}Nd (Table 5). While Ce oxidation on Ln-Spec resins typically uses $NaBrO_3$ as a strong oxidizing agent[30,89], tests with H_2O_2 should be performed by groups using the $NaBrO_3$ method. Indeed, in the event that H_2O_2 is not affecting the affinity of other REEs for the Ln-Spec resins, it would provide a way to achieve lower blanks and circumvent the need for a clean-up chemistry to remove Na and/or Br from the purified Nd cut.

In eliminating Sm interference on ^{144}Nd, tests conducted with the multielement Spex solution suggested that two passes through the α-HIBA column may suffice in reducing ^{144}Sm to near-sub-ppm levels for most basaltic and granitic compositions and samples whose Sm/Nd ratios are generally within a factor of two of chondritic values (Table 4). The degree of purity achieved for BHVO-2 and Columbia River Basalt (Table 5) confirms these expectations, with interference levels on ^{144}Nd ranging from 0.5 to 2.5 ppm. Due to tailing of Sm into the Nd cut, the purification is not as good as for Ce, yet it is sufficient for accurate interference correction and for achieving ±2 ppm precision on $^{142}Nd/^{144}Nd$. At these interference levels, $^{148}Nd/^{144}Nd$ and $^{150}Nd/^{144}Nd$ measurements of BHVO-2 and Columbia River Basalt were also reproducible at the level of precision for static measurements with the TIMS (Table 5). Eliminating ^{144}Sm to sub-ppm levels may require a third pass on α-HIBA for samples characterized by light REE depletion, such as clinopyroxenes and garnet-rich rocks.

Instabilities in elution conditions might affect the quality of the separation, as suggested by the late release of (i) Sm during the elution of Nd and Ce, and (ii) Nd during the elution of Ce, during the experiment conducted using a flared Teflon nozzle (Figure 5). The main effect of the shape of the flared nozzle was that it hindered the formation of small (~50 µL) drops at the bottom of the column. Instead, surface tension tended to maintain the eluate inside the nozzle, creating a small amount of back pressure that was periodically released with every drop eventually formed. The larger drop volume can be seen in the apparently earlier elution (i.e., lower drop number) of Sm, Nd and Ce (Figure 5a) relative to the reference elution (Figure 5b), where a straight nozzle was used. The periodic changes in pressurization of the column induced by the formation of these larger drops, could have impacted the compaction of the resin, and therefore the eluent flow path, resulting in more pronounced and longer elution tails for each element.

If correct, this hypothesis suggests that parameters leading to back-pressure in the column (*e.g.*, low frit porosity, resin with low particle size) may result in similarly poor separations. While more work would be necessary to fully explore this idea, the problem was solved by replacing the flared nozzle with one that was well-machined (Figure 5b, top right corner).

A related potential issue is the fact that column pressurization will result in some decrease in resin porosity over the duration of the elution. This may lead to shifts in elution peak positions, as porosity is a factor that affects plate height. To minimize the compaction of the resin, a high-porosity frit is recommended, which enables a reasonable flow rate for the duration of the chemistry. In our case, we found that a 35 µm frit was optimal, where a pressure of 0.35 psi for a 2 mm ID, 30-cm long column was sufficient to create a slow and steady flow, achieving high yields. By pressurizing the column consistently from run to run, changes in peak position can be successfully avoided and the calibration remains robust and reliable.

An optimized, scalable set-up

Based on the results described and discussed above, an optimized protocol was established and is summarized in Figure 8. This protocol is relevant to the column dimensions used in this study (see full details in Supplementary Materials). Although each column needs to be individually calibrated to account for small differences in column dimensions, the setup is scalable. When setting up multiple pressurized α-HIBA columns, paying attention to the following details will help ensure homogeneity/consistency in flow and applied pressure. (i) Tubing diameters should be larger near the compressed air source and decrease to smaller diameters toward the direction of the columns. (ii) Wye-connectors are recommended to ensure identical pressurization of each branch. (iii) To ensure pressure consistency across multiple columns, tubing of equal length should be used to set up each column. (iv) The α-HIBA columns should be set up in a dedicated area to avoid disturbances to the columns or pressurization tubing, and ensure stable elution conditions.

Conclusions

We present the results of a series of tests aimed at refining the α-HIBA column chromatography method used to purify Nd for high-precision isotope analyses. We find that this method is capable to produce consistently high yields (>95%) and extremely good separation of Ce, Pr and Sm from Nd, provided stable elution conditions are maintained, and elution flow rates are kept low enough to enable full equilibration of the analytes between the mobile and the solid phase. The timescale for sample purification is ~4 days, and multiple samples can be processed in parallel.

Using this optimized method, we report high-precision data on a geostandard and a terrestrial sample to show that our protocol does not result in any resolvable systematic bias, within the precision of our measurements (*e.g.*, ±2ppm on $^{142}Nd/^{144}Nd$). The full details on the experimental setup are presented here and in the Supplementary Materials, to facilitate knowledge transfer and installation in other laboratories.

Conflicts of interest

The authors have no conflicts to declare.

Acknowledgements

The authors thank S. B. Jacobsen for useful conversations about glass column material. This work was supported by a Walter De Logi grant from Caltech for 2019-2021, NSF-EAR grant 1824002, as well as start-up funds provided by Caltech to FLHT.

Author Contributions

Eugenia Hyung: Conceptualization, Data curation, Investigation, Formal analysis, Methodology, Visualization, Writing – original draft. **François L.H. Tissot:** Conceptualization, Funding acquisition, Project administration, Resources, Supervision, Validation, Visualization, Writing – review and editing.

References

1 A. Friedman, *Radiochim. Acta*, 1966, **5**, 192–194.

2 D. Papanastassiou, D. DePaolo and G. Wasserburg, *Proc. Lunar Planet. Sci. Conf. 8th*, 1977, 1639–1672.

3 R. W. Carlson, L. E. Borg, A. M. Gaffney and M. Boyet, *Philos. Trans. R. Soc. A Math. Phys. Eng. Sci.*, 2014, **372**, 1–21.

4 E. J. Chin, C.-T. A. Lee and J. Blichert-Toft, *Geochemical Perspect. Lett.*, 2015, **1**, 20–32.

5 W. M. White and A. W. Hofmann, *Nature*, 1982, **296**, 821–825.

6 A. W. Hofmann, *Nature*, 1997, **385**, 219–229.

7 A. W. Hofmann, in *Treatise on Geochemistry: Second Edition*, 2003, pp. 61–101.

8 S. B. Jacobsen and G. J. Wasserburg, *Earth Planet. Sci. Lett.*, 1980, **50**, 139–155.

9 S. B. Jacobsen, J. E. Quick and G. J. Wasserburg, *Earth Planet. Sci. Lett.*, 1984, **68**, 361–378.

10 G. Caro, B. Bourdon, J.-L. Birck and S. Moorbath, *Nature*, 2003, **423**, 428–432.

11 G. Caro, B. Bourdon, J.-L. Birck and S. Moorbath, *Geochim. Cosmochim. Acta*, 2006, **70**, 164–191.

12 V. Debaille, A. D. Brandon, Q. Z. Yin and B. Jacobsen, *Nature*, 2007, **450**, 525–528.

13 A. D. Brandon, T. J. Lapen, V. Debaille, B. L. Beard, K. Rankenburg and C. Neal, *Geochim. Cosmochim. Acta*, 2009, **73**, 6421–6445.

14 G. Caro, P. Morino, S. J. Mojzsis, N. L. Cates and W. Bleeker, *Earth Planet. Sci. Lett.*, 2017, **457**, 23–37.

15 N. S. Saji, K. Larsen, D. Wielandt, M. Schiller, M. M. Costa, M. J. Whitehouse, M. T. Rosing and M. Bizzarro, *Geochemical Perspect. Lett.*, 2018, **7**, 43–48.

16 M. T. McCulloch and G. J. Wasserburg, *Astrophys. J.*, 1978, **220**, 15–19.

17 L. Qin, R. W. Carlson and C. M. O. Alexander, *Geochim. Cosmochim. Acta*, 2011, **75**, 7806–7828.

18 Q. R. Shollenberger, L. E. Borg, J. Render, S. Ebert, A. Bischoff, S. S. Russell and G. A. Brennecka, *Geochim. Cosmochim. Acta*, 2018, **228**, 62–80.

19 M. Boyet and A. Gannoun, *Geochim. Cosmochim. Acta*, 2013, **121**, 652–666.

20 G. A. Brennecka, L. E. Borg and M. Wadhwa, *Proc. Natl. Acad. Sci.*, 2013, **110**, 17241–17246.

21 A. Bouvier and M. Boyet, *Nature*, 2016, **537**, 399–402.

22 C. Burkhardt, L. E. Borg, G. A. Brennecka, Q. R. Shollenberger, N. Dauphas and T. Kleine, *Nature*, 2016, **537**, 394–398.

23 J. Render, M. Fischer-Gödde, C. Burkhardt and T. Kleine, *Geochemical Perspect. Lett.*, 2017, **3**, 170–178.

24 R. Fukai and T. Yokoyama, *Astrophys. J.*, 2019, **879**, 1–12.

25 P. Frossard, Z. Guo, M. Spencer, M. Boyet and A. Bouvier, *Earth Planet. Sci. Lett.*, 2021, **566**, 116968.

26 C. L. J. Harper and S. B. Jacobsen, *Nature*, 1992, **360**, 726–732.

27 E. Hyung and S. B. Jacobsen, *Proc. Natl. Acad. Sci.*, 2020, **117**, 14738–14744.

28 N. S. Saji, D. Wielandt, C. Paton and M. Bizzarro, *J. Anal. At. Spectrom.*, 2016, **31**, 1490–1504.

29 B. J. Peters, J. M. D. Day and L. A. Taylor, *Earth Planet. Sci. Lett.*, 2016, **448**, 150–160.

30 M. Garçon, M. Boyet, R. W. Carlson, M. F. Horan, D. Auclair and T. D. Mock, *Chem. Geol.*, 2018, **476**, 493–514.

31 K. L. Nash and M. P. Jensen, *Sep. Sci. Technol.*, 2001, **36**, 1257–1282.

32 G. R. Choppin and R. J. Silva, *J. Inorg. Nucl. Chem.*, 1956, **3**, 153–154.

33 G. W. Lugmair, N. B. Scheinin and K. Marti, *Proc. 6th Lunar Sci. Conf.*, 1975, 1419–1429.

34 D. J. DePaolo and G. J. Wasserburg, *Geophys. Res. Lett.*, 1976, **3**, 3–6.

35 H. G. Stosch, R. W. Carlson and G. W. Lugmair, *Earth Planet. Sci. Lett.*, 1980, **47**, 1–22.

36 K. Ishizaka and R. W. Carlson, *Earth Planet. Sci. Lett.*, 1983, **64**, 327–340.

37 R. W. Carlson, *Geochim. Cosmochim. Acta*, 1984, **48**, 2357–

2372.

38 S. B. Jacobsen and G. J. Wasserburg, *Earth Planet. Sci. Lett.*, 1984, **67**, 137–150.

39 S. B. Jacobsen and R. F. Dymek, *J. Geophys. Res. Solid Earth*, 1988, **93**, 338–354.

40 R. J. Walker, R. W. Carlson, S. B. Shirey and F. R. Boyd, *Geochim. Cosmochim. Acta*, 1989, **53**, 1583–1595.

41 S. W. Nicholson and S. B. Shirey, *J. Geophys. Res.*, 1990, **95**, 10851–10868.

42 K. Tu, M. F. J. Flower, R. W. Carlson, G. Xie, C.-Y. Chen and M. Zhang, *Chem. Geol.*, 1992, **97**, 47–63.

43 S. B. Shirey, K. W. Klewin, J. H. Berg and R. W. Carlson, *Geochim. Cosmochim. Acta*, 1994, **58**, 4475–4490.

44 L. E. Nyquist, H. Wiesmann, B. Bansal, C.-Y. Shih, J. E. Keith and C. L. Harper, *Geochim. Cosmochim. Acta*, 1995, **59**, 2817–2837.

45 D. G. Pearson, S. B. Shirey, R. W. Carlson, F. R. Boyd, N. P. Pokhilenko and N. Shimizu, *Geochim. Cosmochim. Acta*, 1995, **59**, 959–977.

46 H. Nguyen, M. F. J. Flower and R. W. Carlson, *Geochim. Cosmochim. Acta*, 1996, **60**, 4329–4351.

47 L. E. Borg, L. E. Nyquist, L. A. Taylor, H. Wiesmann and C.-Y. Shih, *Geochim. Cosmochim. Acta*, 1997, **61**, 4915–4931.

48 E. Widom, R. W. Carlson, J. B. Gill and H.-U. Schmincke, *Chem. Geol.*, 1997, **140**, 49–68.

49 L. Borg, M. Norman, L. Nyquist, D. Bogard, G. Snyder, L. Taylor and M. Lindstrom, *Geochim. Cosmochim. Acta*, 1999, **63**, 2679–2691.

50 M. Boyet, J. Blichert-Toft, M. Rosing, M. Storey, P. Telouk and F. Albarede, *Earth Planet. Sci. Lett.*, 2003, **214**, 427–442.

51 C. M. Petrone, L. Francalanci, R. W. Carlson, L. Ferrari and S. Conticelli, *Chem. Geol.*, 2003, **193**, 1–24.

52 L. E. Borg, C. K. Shearer, Y. Asmerom and J. J. Papike, *Nature*, 2004, **432**, 209–211.

53 R. W. Carlson, A. J. Irving, D. J. Schulze and B. C. Hearn, *Lithos*, 2004, **77**, 453–472.

54 H. D. Scher and E. E. Martin, *Earth Planet. Sci. Lett.*, 2004, **228**, 391–405.

55 L. E. Borg, J. E. Edmunson and Y. Asmerom, *Geochim. Cosmochim. Acta*, 2005, **69**, 5819–5830.

56 M. Boyet and R. W. Carlson, *Science (80-.).*, 2005, **309**, 576–581.

57 R. W. Carlson, G. Czamanske, V. Fedorenko and I. Ilupin, *Geochemistry, Geophys. Geosystems*, 2006, **7**, 1–21.

58 R. W. Carlson, M. Boyet and M. Horan, *Science (80-.).*, 2007, **316**, 1175–1178.

59 A. M. Gaffney, L. E. Borg and Y. Asmerom, *Geochim. Cosmochim. Acta*, 2007, **71**, 3656–3671.

60 J. O'Neil, R. W. Carlson, D. Francis and R. K. Stevenson, *Science (80-.).*, 2008, **321**, 1828–1832.

61 L. E. Borg, A. M. Gaffney, C. K. Shearer, D. J. DePaolo, I. D. Hutcheon, T. L. Owens, E. Ramon and G. Brennecka, *Geochim. Cosmochim. Acta*, 2009, **73**, 3963–3980.

62 J. Edmunson, L. E. Borg, L. E. Nyquist and Y. Asmerom, *Geochim. Cosmochim. Acta*, 2009, **73**, 514–527.

63 J. Harvey and E. F. Baxter, *Chem. Geol.*, 2009, **258**, 251–257.

64 D. Upadhyay, E. E. Scherer and K. Mezger, *Nature*, 2009, **459**, 1118–1121.

65 L. E. Borg, J. N. Connelly, M. Boyet and R. W. Carlson, *Nature*, 2011, **477**, 70–73.

66 A. Cipriani, E. Bonatti and R. W. Carlson, *Geochemistry, Geophys. Geosystems*, 2011, **12**, 1–8.

67 A. M. Gaffney, L. E. Borg, Y. Asmerom, C. K. Shearer and P. V. Burger, *Meteorit. Planet. Sci.*, 2011, **46**, 35–52.

68 A. Gannoun, M. Boyet, H. Rizo and A. El Goresy, *Proc. Natl. Acad. Sci.*, 2011, **108**, 7693–7.

69 J. Liu, R. W. Carlson, R. L. Rudnick, R. J. Walker, S. Gao and F. Wu, *Chem. Geol.*, 2012, **332–333**, 1–14.

70 J. O'Neil, R. W. Carlson, J.-L. Paquette and D. Francis, *Precambrian Res.*, 2012, **220–221**, 23–44.

71 H. Rizo, M. Boyet, J. Blichert-Toft, J. O'Neil, M. T. Rosing and J.-L. Paquette, *Nature*, 2012, **491**, 96–100.

72 S. Wakaki and T. Tanaka, *Int. J. Mass Spectrom.*, 2012, **323–324**, 45–54.

73 I. S. Puchtel, J. Blichert-Toft, M. Touboul, R. J. Walker, G. R. Byerly, E. G. Nisbet and C. R. Anhaeusser, *Geochemica Cosmochem. Acta*, 2013, **108**, 63–90.

74 H. Rizo, M. Boyet, J. Blichert-Toft and M. T. Rosing, *Earth Planet. Sci. Lett.*, 2013, **377–378**, 324–335.

75 S. M. Elardo, C. K. Shearer, A. L. Fagan, L. E. Borg, A. M. Gaffney, P. V. Burger, C. R. Neal, V. A. Fernandes and F. M. McCubbin, *Meteorit. Planet. Sci.*, 2014, **49**, 261–291.

76 N. E. Marks, L. E. Borg, I. D. Hutcheon, B. Jacobsen and R. N. Clayton, *Earth Planet. Sci. Lett.*, 2014, **405**, 15–24.

77 M. Boyet, R. W. Carlson, L. E. Borg and M. Horan, *Geochim. Cosmochim. Acta*, 2015, **148**, 203–218.

78 L. E. Borg, G. A. Brennecka and S. J. K. Symes, *Geochim. Cosmochim. Acta*, 2016, **175**, 150–167.

79 J. O'Neil, H. Rizo, M. Boyet, R. W. Carlson and M. T. Rosing, *Earth Planet. Sci. Lett.*, 2016, **442**, 194–205.

80 I. S. Puchtel, J. Blichert-Toft, M. Touboul, M. F. Horan and R. J. Walker, *Geochemistry Geophys. Geosystems*, 2016, **17**, 2825–2834.

81 I. S. Puchtel, M. Touboul, J. Blichert-Toft, R. Walker, A. Brandon, R. Nicklas, V. Kulikov and A. Samsonov, *Geochemica Cosmochem. Acta*, 2016, **180**, 227–255.

82 L. E. Borg, J. N. Connelly, W. Cassata, A. M. Gaffney and M. Bizzarro, *Geochim. Cosmochim. Acta*, 2017, **201**, 377–391.

83 I. Gautam, J. S. Ray, R. Bhutani, S. Balakrishnan and J. K. Dash, *Chem. Geol.*, 2017, **466**, 479–490.

84 J. M. Maya, R. Bhutani, S. Balakrishnana and S. Rajee Sandhya, *Geosci. Front.*, 2017, **8**, 467–481.

85 N. Bellot, M. Boyet, R. Doucelance, P. Bonnand, I. P. Savov, T. Plank and T. Elliott, *Chem. Geol.*, 2018, **500**, 46–63.

86 L. E. Borg, W. S. Cassata, J. Wimpenny, A. M. Gaffney and C. K. Shearer, *Geochim. Cosmochim. Acta*, 2020, **290**, 312–332.

87 C. K. Sio, L. E. Borg and W. S. Cassata, *Earth Planet. Sci. Lett.*, 2020, **538**, 116219.

88 P. Richard, N. Shimizu and C. J. Allègre, *Earth Planet. Sci. Lett.*, 1976, **31**, 269–278.

89 M. Rehkämper, M. Gärtner, S. J. G. Galer and S. L. Goldstein, *Chem. Geol.*, 1996, **129**, 201–208.

90 C. Pin and J. F. Santos Zalduegui, *Anal. Chim. Acta*, 1997, **339**, 79–89.

91 J. Blichert-Toft, M. Boyet, P. Telouk and F. Albarede, *Earth Planet. Sci. Lett.*, 2002, **204**, 167–181.

92 F. A. Frey, S. Huang, J. Blichert-Toft, M. Regelous and M. Boyet, *Geochemistry Geophys. Geosystems*, 2005, **6**, 1–23.

93 H. Tazoe, H. Obata and T. Gamo, *J. Anal. At. Spectrom.*, 2007, **22**, 616–622.

94 D. T. Murphy, A. D. Brandon, V. Debaille, R. Burgess and C. Ballentine, *Geochim. Cosmochim. Acta*, 2010, **74**, 738–750.

95 H. Rizo, M. Boyet, J. Blichert-Toft and M. Rosing, *Earth Planet. Sci. Lett.*, 2011, **312**, 267–279.

96 H. Tazoe, H. Obata and T. Gamo, *Geochemistry Geophys. Geosystems*, 2011, **12**, 1–14.

97 Y. Hirahara, Q. Chang, T. Miyazaki, T. Takahashi and J.-I. Kimura, *JAMSTEC Rep. Res. Dev.*, 2012, **15**, 27–33.

98 F. Lacan, K. Tachikawa and C. Jeandel, *Chem. Geol.*, 2012, **300–301**, 177–184.

99 T. van de Flierdt, K. Pahnke, H. Amakawa, P. Andersson, C. Basak, B. Coles, C. Colin, K. Crocket, M. Frank, N. Frank, S. L. Goldstein, V. Goswami, B. A. Haley, E. C. Hathorne, S. R. Hemming, G. M. Henderson, C. Jeandel, K. Jones, K. Kreissig, F. Lacan, M. Lambelet, E. E. Martin, D. R. Newkirk, H. Obata, L. Pena, A. M. Piotrowski, C. Pradoux, H. D. Scher, H. Schoberg, S. K. Singh, T. Stichel, H. Tazoe, D. Vance and J. Yang, *Limnol. Oceanogr. Methods*, 2012, **10**, 234–251.

100 V. Debaille, C. O'Neill, A. D. Brandon, P. Haenecour, Q.-Z. Yin, N. Mattielli and A. H. Treiman, *Earth Planet. Sci. Lett.*, 2013, **373**, 83–92.

101 T. J. Ireland, F. L. H. Tissot, R. Yokochi and N. Dauphas, *Chem. Geol.*, 2013, **357**, 203–214.

102 A. S. G. Roth, B. Bourdon, S. J. Mojzsis, M. Touboul, P. Sprung, M. Guitreau and J. Blichert-Toft, *Earth Planet. Sci. Lett.*, 2013, **361**, 50–57.

103 C. L. McLeod, A. D. Brandon and R. M. G. Armytage, *Earth Planet. Sci. Lett.*, 2014, **396**, 179–189.

104 C.-F. Li, X.-C. Wang, Y.-L. Li, Z.-Y. Chu, J.-H. Guo and X.-H. Li, *J. Anal. At. Spectrom.*, 2015, **30**, 895–902.

105 S. Kagami and T. Yokoyama, *Anal. Chim. Acta*, 2016, **937**, 151–159.

106 R. Fukai and T. Yokoyama, *Earth Planet. Sci. Lett.*, 2017, **474**, 206–214.

107 M. Boyet, A. Bouvier, P. Frossard, T. Hammouda, M. Garçon and A. Gannoun, *Earth Planet. Sci. Lett.*, 2018, **488**, 68–78.

108 M. F. Horan, R. W. Carlson, R. J. Walker, M. Jackson, M. Garçon and M. Norman, *Earth Planet. Sci. Lett.*, 2018, **484**, 184–191.

109 K. P. Schneider, J. E. Hoffmann, M. Boyet, C. Munker and A. Kroner, *Earth Planet. Sci. Lett.*, 2018, **487**, 54–66.

110 P. Bonnand, R. Doucelance, M. Boyet, P. Bachèlery, C. Bosq, D. Auclair and P. Schiano, *Earth Planet. Sci. Lett.*, 2020, **532**, 116028.

111 C. Israel, M. Boyet, R. Doucelance, P. Bonnand, P. Frossard, D. Auclair and A. Bouvier, *Earth Planet. Sci. Lett.*, 2020, **530**, 115941.

112 N. Sivaraman, R. Kumar, S. Subramaniam and P. R. Vasudeva Rao, *J. Radioanal. Nucl. Chem.*, 2002, **252**, 491–495.

113 N. S. Saji, D. Wielandt, J. C. Holst and M. Bizzarro, *Geochim. Cosmochim. Acta*, 2020, **281**, 135–148.

114 J. Y. Hu, N. Dauphas, F. L. H. Tissot, R. Yokochi, T. J. Ireland, Z. Zhang, A. M. Davis, F. J. Ciesla, L. Grossman, B. L. A. Charlier, M. Roskosz, E. E. Alp, M. Y. Hu and J. Zhao, *Sci. Adv.*, 2021, **7**, 22–28.

115 C. Pin and A. Gannoun, *J. Anal. At. Spectrom.*, 2019, **13**, 310–318.

116 L. E. Borg, A. M. Gaffney, T. S. Kruijer, N. A. Marks, C. K. Sio and J. Wimpenny, *Earth Planet. Sci. Lett.*, 2019, **523**, 115706.

117 G. P. Russ III, D. S. Burnett, R. E. Lingenfelter and G. J. Wasserburg, *Earth Planet. Sci. Lett.*, 1971, **13**, 53–60.

118 O. Eugster, F. Tera, D. S. Burnett and G. J. Wasserburg, *J. Geophys. Res.*, 1970, **75**, 2753–2768.

119 M. F. Al-Hakkani, *SN Appl. Sci.*, 2019, **1**, 1–15.

120 A. J. P. Martin and R. L. M. Synge, *Biochem. J.*, 1941, **35**, 1358–1368.

121 J. J. van Deemter, F. J. Zuiderweg and A. Klinkenberg, *Chem. Eng. Sci.*, 1956, **6**, 271–289.

122 D. C. Harris, in *Quantitative Chemical Analysis*, W.H. Freeman and Company, New York, 8th edn., 2015, pp. 537–558.

123 H. Li, F. L. H. Tissot, S.-G. Lee, E. Hyung and N. Dauphas, *ACS Earth Sp. Chem.*, 2021, **5**, 55–65.

ARTICLE

Table 1. Elution scheme for Nd separation

Step I. Major element-REE separation (Bio-Rad AG50X8 resin, 100–200 mesh)

Step	Volume (mL)	Eluent
Rinse with 30 mL 4 M HCl		
Condition resin	5	1.5 M HCl
Load sample	3	1.5 M HCl
Rinse major elements	3	1.5 M HCl
	6 + 49	2.0 M HCl
Precollection Nd	3	4.0 M HCl
Collect Nd	30	4.0 M HCl
Postcollection Nd	3	4.0 M HCl
Rinse with 30 mL 4 M HCl, or discard resin		

Step II. Nd purification process (Bio-Rad AG50X4 resin, 200–400 mesh) performed twice

Step	Volume	Eluent
Condition resin	7 mL	pH = 4.6, α-HIBA
Load sample	150 μL	0.75 M HCl
Discard	0–39 drops	pH = 4.6, α-HIBA
Collect Sm	40–60 drops	pH = 4.6, α-HIBA
Discard	59–84 drops	pH = 4.6, α-HIBA
Collect Nd	85–118 drops	pH = 4.6, α-HIBA
Discard resin		

Table 2. Cup configuration for a 2-sequence dynamic run.

	Faraday cup									Zoom optics	
	L4	L3	L2	L1	Ax	H1	H2	H3	H4	Focus (V)	Dispersion (V)
Sequence 1	^{140}Ce	^{141}Pr	^{142}Nd	^{143}Nd	^{144}Nd	^{145}Nd	^{146}Nd	^{147}Sm	^{148}Nd	0	0
Sequence 2	^{142}Nd	^{143}Nd	^{144}Nd	^{145}Nd	^{146}Nd	^{147}Sm	^{148}Nd		^{150}Nd	0	-9.0

Table 3. Drop rate vs. yield comparison (α-HIBA column, single pass)

Column length	Relative flow rates			
	Fast		Slow	
	pressure	yield	pressure	yield
30 cm	1.0 psi	93.5%	0.35 psi	98.5%
60 cm	2.2 psi	70.0%	1.5 psi	96.8%

Table 4. Isobaric interferences after α-HIBA chemistry at a flow rate of 29.9 µL/min

Sample type	Ratio^{+}	Pre-chemistry	After 1st pass	After 2nd pass§
Spex§§	Ce/Nd	1.0	1.14E-03	1.30E-06
	^{142}Ce/^{142}Nd			5.47E-07
Spex*	Ce/Nd	1.0	4.54E-05	<1e-7
	^{142}Ce/^{142}Nd			<1e-8
Spex	Pr/Nd	1.0	3.00E-02	9.00E-04
Spex	Sm/Nd	1.0	3.60E-03	1.30E-05
	^{144}Sm/^{144}Nd			1.61E-06
Chondrite‡	Sm/Nd‡	0.324‡	1.50E-04	4.20E-06
	^{144}Sm/^{144}Nd			5.20E-07

Spex: Multi-elemental solution containig all REEs, Sc, Y, and Th in equal proportion.

$^{+}$Elemental ratios are weight ratios. Isotopic ratios are atomic ratios.

§Calculated based on decrease in 1st pass

§§Not treated with H_2O_2 prior to loading

*Treated with 30% H_2O_2 prior to loading to oxidize Ce

‡Calculated assuming a chondritic value from McDonough and Sun (1995) and based on the results on Spex solution

Table 5. Nd isotope data for the unprocessed JNdi-1 standard and two reference materials processed through chemsitry.

	^{142}Nd beam intensity	Number of cycles	^{142}Ce/^{142}Nd (ppm)	^{144}Sm/^{144}Nd (ppm)	^{142}Nd/^{144}Nd(2σ) dynamic (ppm)	^{143}Nd/^{144}Nd(2σ) static (ε)	^{145}Nd/^{144}Nd(2σ) static (ppm)	^{148}Nd/^{144}Nd(2σ) static (ppm)	^{150}Nd/^{144}Nd(2σ) static (ppm)
JNdi-1	7 V	450			-0.1(2.8)	-10.42(0.03)	-2.2(2.9)	14.3(5.3)	-0.4(7.5)
JNdi-1	7 V	900			-0.4(2.2)	-10.32(0.02)	2.1(1.9)	9.2(3.7)	1.0(5.3)
JNdi-1	7 V	720			0.1(2.5)	-10.40(0.03)	0.2(2.8)	11.0(4.7)	8.5(6.9)
JNdi-1	7 V	900			-1.5(2.3)	-10.38(0.02)	-0.6(2.0)	3.5(3.7)	-18.0(5.0)
JNdi-1	7 V	900			0.8(2.0)	-10.40(0.02)	-2.3(2.1)	12.9(3.7)	-5.9(5.1)
JNdi-1	7 V	900			-1.2(2.4)	-10.34(0.02)	4.6(2.3)	-11.7(3.9)	7.0(5.0)
JNdi-1	7 V	720			-1.4(2.3)	-10.43(0.02)	0.9(2.0)	-13.9(3.9)	10.1(5.3)
JNdi-1	7 V	900			2.1(2.2)	-10.39(0.02)	-0.5(2.2)	-8.1(3.7)	17.0(5.3)
JNdi-1	7 V	900			0.8(2.1)	-10.40(0.02)	0.3(2.1)	-12.4(4.2)	0.9(5.7)
JNdi-1	7 V	1260			0.8(1.7)	-10.43(0.02)	-2.5(1.8)	-4.7(3.0)	-20.3(4.8)
Average					**0(2.4)**	**-10.39(0.04)**	**0(4.4)**	**0(22.7)**	**0(23.9)**
BHVO-2#1-1	4 V	720	0.077	0.49	-2.1(3.6)	6.60(0.04)	1.5(3.2)	-16.3(5.9)	29.5(7.8)
BHVO-2#1-2	7 V	360	0.3	1	0.9(5.0)	6.58(0.03)	-1.2(3.2)	4.0(5.8)	3.1(8.1)
Average					**-0.6**	**6.59**	**0.2**	**-6.2**	**16.3**
BCR #1-1	6.5 V	540	0.1	2.5	0.1(2.8)	-0.18(0.03)	-1.0(2.8)	-0.5(4.7)	-11.3(6.7)
BCR #2-1	3 V	900	0.3	0.8	0.0(3.2)	-0.17(0.04)	1.2(3.5)	-10.8(5.6)	14.5(8.6)
BCR #2-2	7 V	900	0.96	1.12	0.2(1.9)	-0.18(0.02)	-1.2(2.0)	-0.3(3.6)	-17.1(5.3)
Average					**0.1**	**-0.18**	**0.3**	**-3.9**	**-4.6**

#1 and #2 denote replicates prepared from different powder digetsion, while '-1' and '2' denote splits of the same solution loaded on different filaments. Ratios and 95% CI are reported in ppm relative to the average JNdi-1 value. ^{143}Nd/^{144}Nd are reported in ε-units relative to the CHUR value of 0.512638 (ref 8).

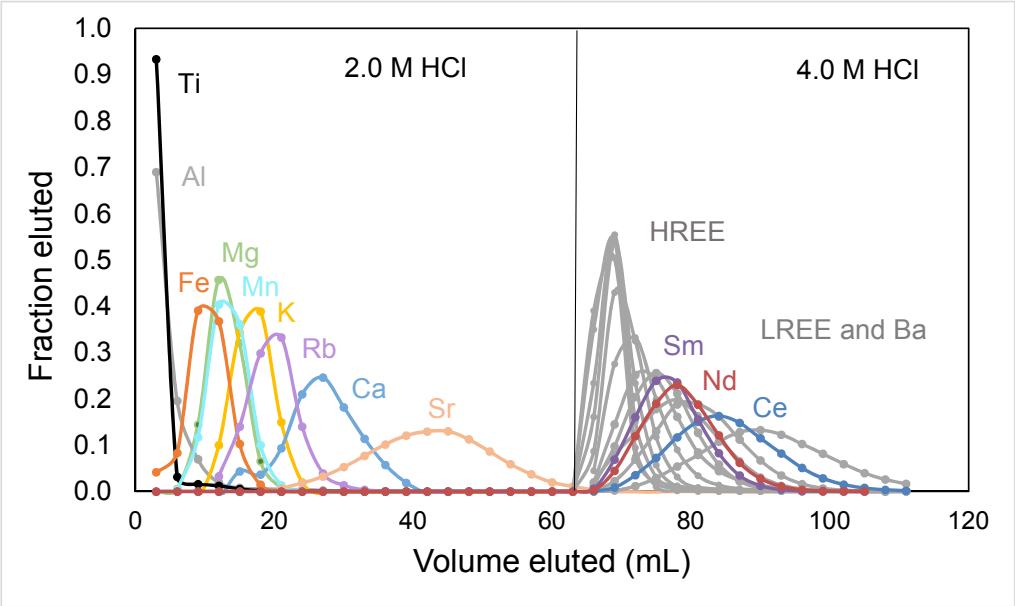

Figure 1. REE-preconcentration elution curve. Samples are loaded in 1.5 M HCl (3 ml per 100 mg of powder digested), most matrix elements are eluted after passing 3 mL of 1.5 M HCl and 55 mL of 2.0 M HCl, and Nd is eluted in 36 mL of 4.0 M HCl (including column tails).

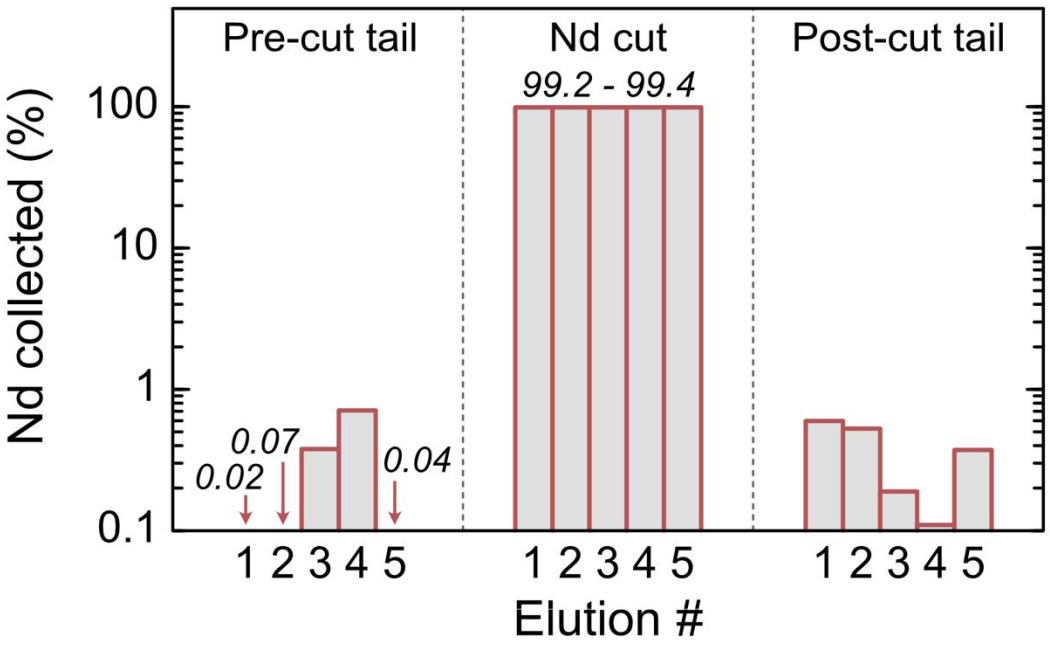

Figure 2. Proportion of Nd collected in the Nd-cut elutions and column tails for multiple elutions on the α-HIBA column, demonstrating the high-consistency of the elution peak position (same drop intervals used in all elutions for all three fractions).

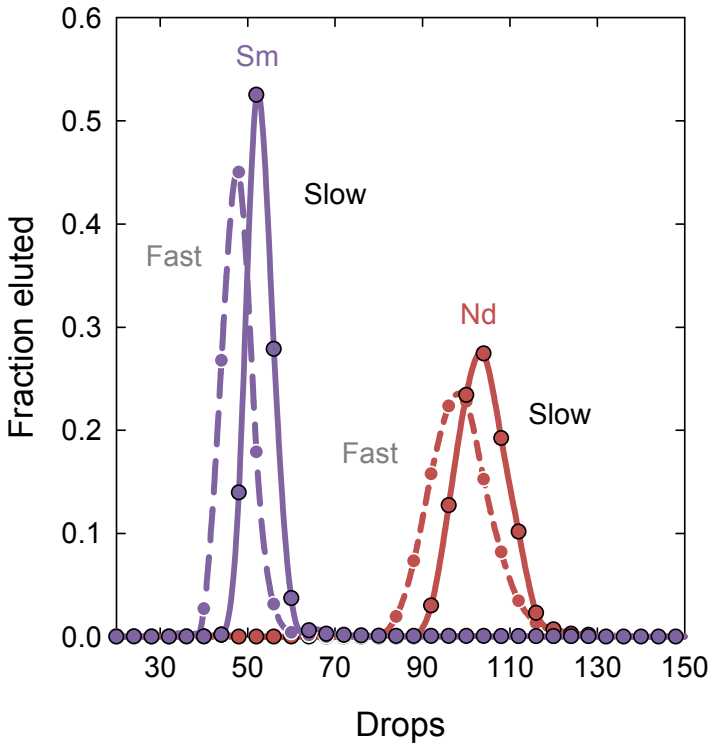

Figure 3. Influence of eluent flow rate on the elution of Sm and Nd on a 30-cm long α-HIBA column: "fast" = 50 µL/min, "slow" = 29.9 µL/min. Although calibrations are highly reproducible for a given drop rate, a slower flow rate results in a narrower cut, allowing for better separation.

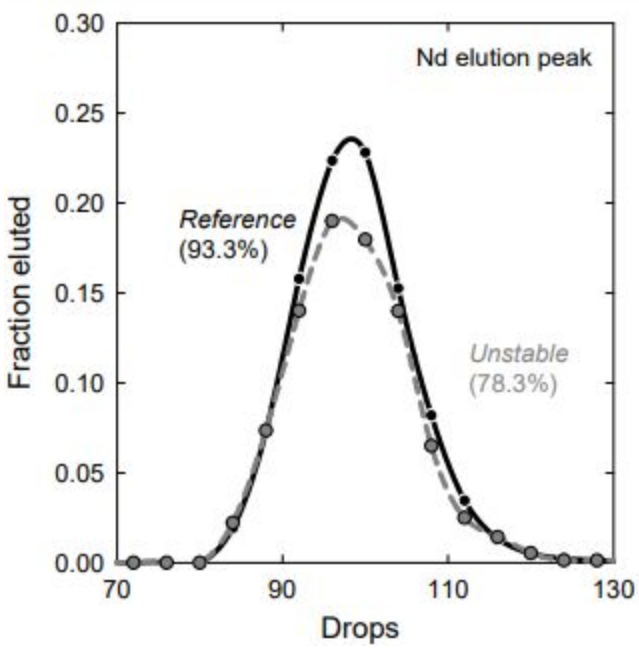

Figure 4. Influence of the stability of elution conditions. Two identical elutions, one free of any disturbance ('*Reference*', yield of 93.3% at a 50 µL/min drop rate), while the pressurization tubing was purposely disturbed during the '*Unstable*' elution. A significantly lower yield (78.3%) is observed in the '*Unstable*' elution, highlighting that importance of stable elution conditions.

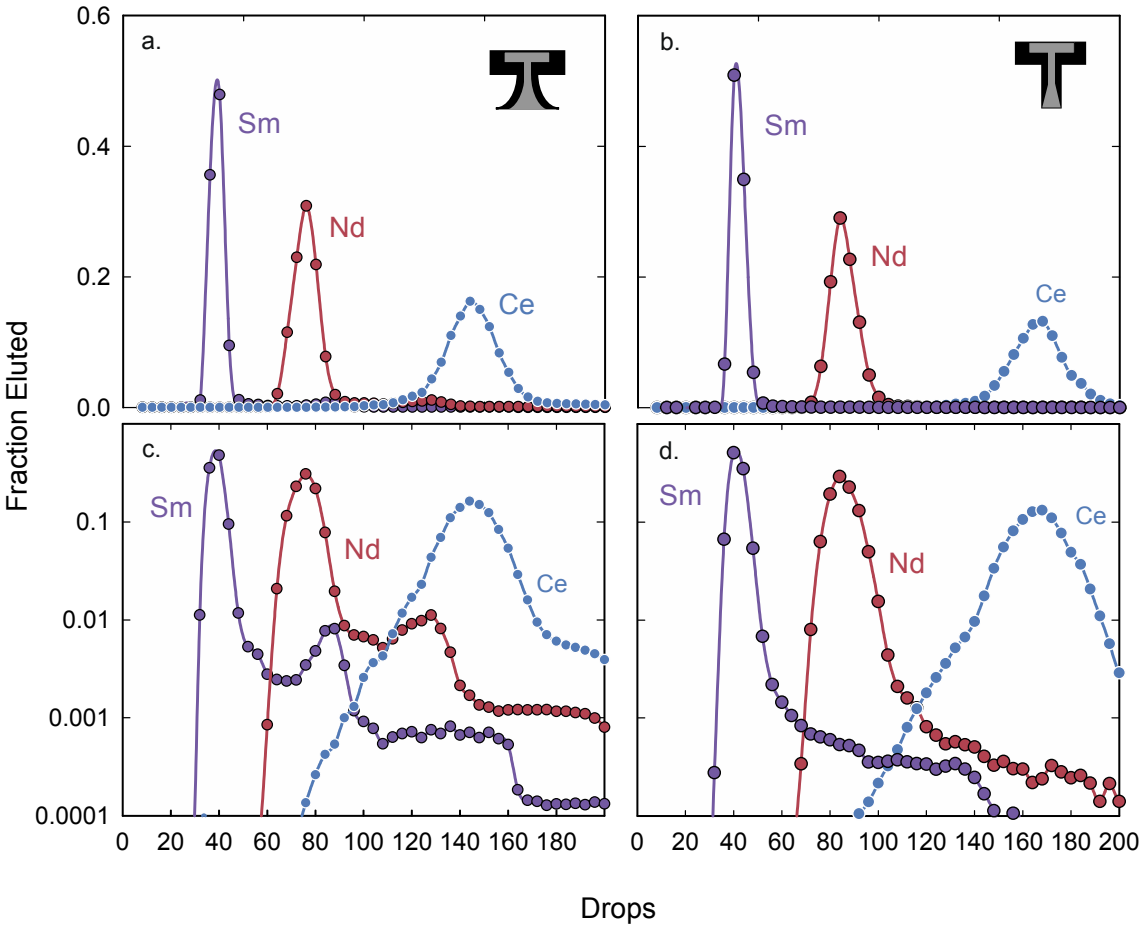

Figure 5. Impact of column end geometry on the elution of Sm, Nd, and Ce on a 30-cm α-HIBA column. (a, c) Elution calibrations using a flared nozzle (top right corner in panel a) *vs.* (b, d) a fixed outer diameter nozzle (top right corner in panel b). Top and bottom panels are in, respectively, linear and log-linear space. Late elemental release occurs with the flared nozzle, possibly due to changes in flow path induced by the periodic back-pressure associated with the formation of larger drops in the flared nozzle.

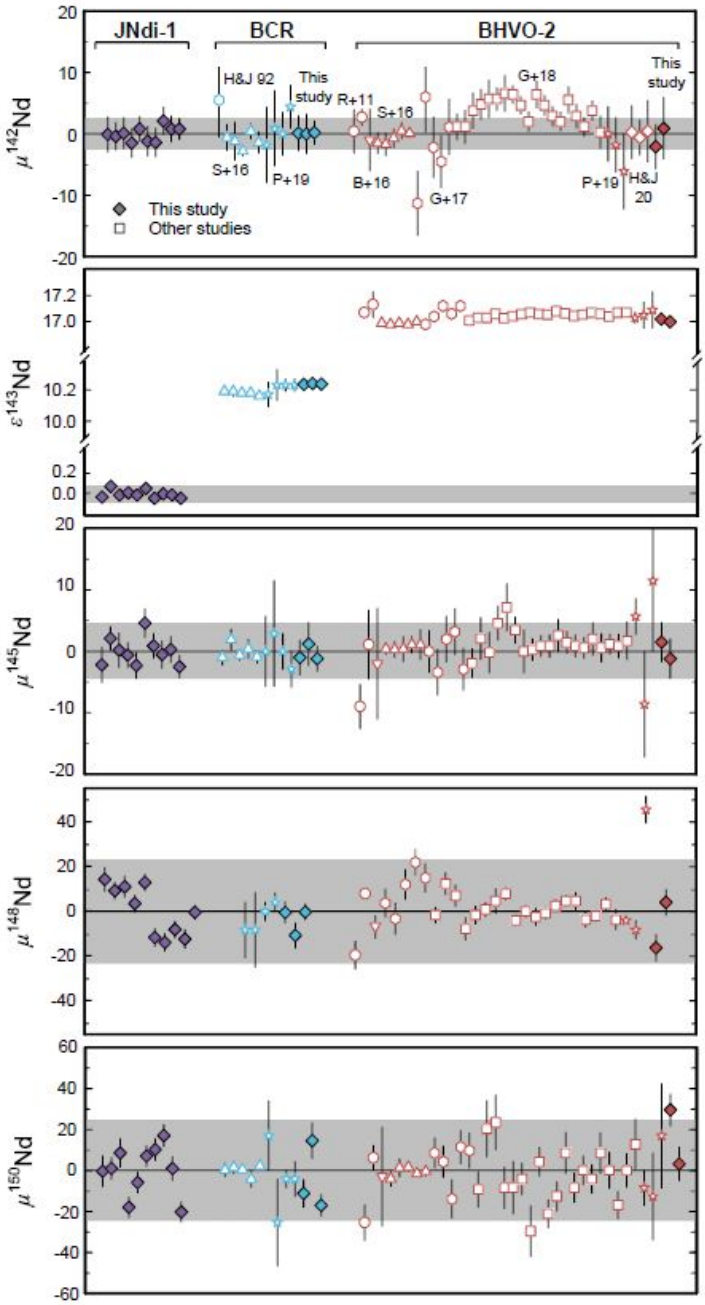

Figure 6. Comparison of Nd isotope data from this study (filled symbols) and literature (open symbols) for the JNdi-1 standard, and two geostandards (BHVO-2, and of Columbia River Basalt). Grey bands show 2σ external reproducibility from this study. Literature data: Harper & Jacobsen (1992) (hexagon with dot), Rizo et al. (2011) (circles), Burkhardt et al., (2016) (downward pointing triangle), Saji et al., (2016) (upward pointing triangle), Gautam et al., (2017) (hexagons), Garcon et al., (2018) (squares), Pin et al., (2019) (stars), and Hyung and Jacobsen (2020) (empty diamonds) (refs. 22,26–28,30,83,95,115). μ = (sample-standard)/standard x 10^6, while ε = (sample-standard)/standard x 10^4 with respect to JNdi-1.

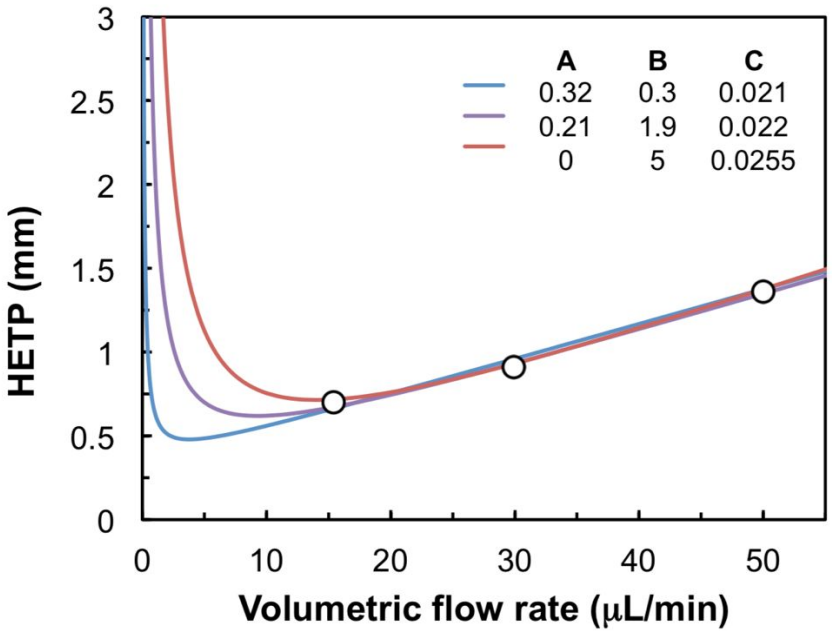

Figure 7. HETP vs flow rate plot, showing the data for three elution rates (circles) on 30 cm α-HIBA columns, and three possible fits to the data (lines) of the van Deemter equation: HETP = A + B/v +Cv. HETP (Eq. 4) were calculated as σ^2/L (ref. 122), where σ is the width (1SD) of the elution peak (assuming a Gaussian curve) scaled to the height of the resin (L). Similar HETP values are inferred using the Nd partition coefficients and simulation chromatography code of Li et al (2021) (ref. 123) and comparing the elutions to modelled elution peaks.

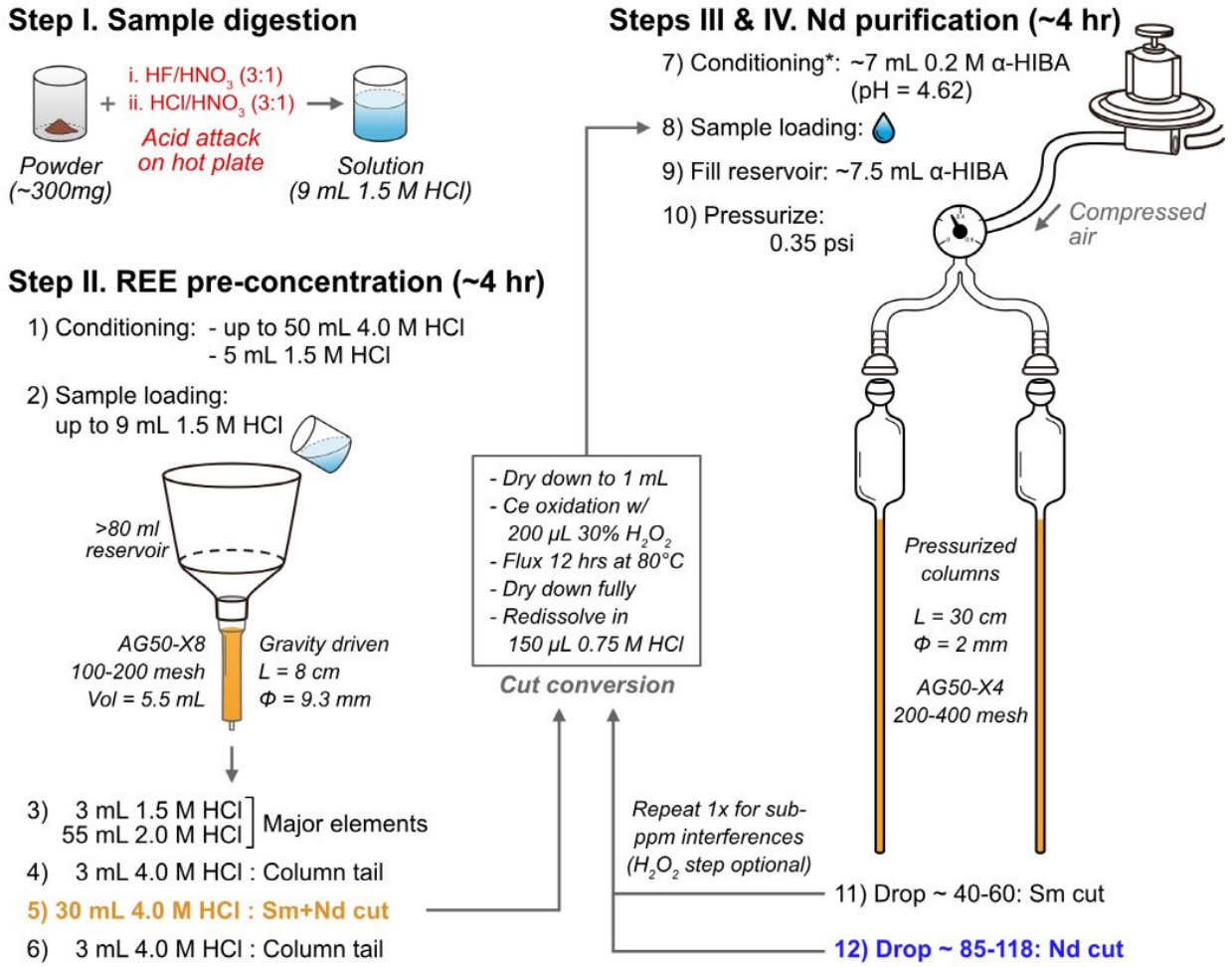

Figure 8. Summary flowchart of the optimized protocol for Nd separation. *Conditioning of the α-HIBA column is gravity driven, and is typically done overnight.